



A scalable method for preparing Cu electrocatalysts that convert CO₂ into C₂₊ products

Taehee Kim ^{1,2} & G. Tayhas R. Palmore ¹✉

Development of efficient catalysts for selective electroreduction of CO₂ to high-value products is essential for the deployment of carbon utilization technologies. Here we present a scalable method for preparing Cu electrocatalysts that favor CO₂ conversion to C₂₊ products with faradaic efficiencies up to 72%. Grazing-incidence X-ray diffraction data confirms that anodic halogenation of electropolished Cu foils in aqueous solutions of KCl, KBr, or KI creates surfaces of CuCl, CuBr, or CuI, respectively. Scanning electron microscopy and energy dispersive X-ray spectroscopy studies show that significant changes to the morphology of Cu occur during anodic halogenation and subsequent oxide-formation and reduction, resulting in catalysts with a high density of defect sites but relatively low roughness. This work shows that efficient conversion of CO₂ to C₂₊ products requires a Cu catalyst with a high density of defect sites that promote adsorption of carbon intermediates and C-C coupling reactions while minimizing roughness.

¹School of Engineering, Brown University, Providence, RI 02912, USA. ²Photo-Electronic Hybrids Research Center, Korea Institute of Science and Technology (KIST), Seoul 02792, Republic of Korea. ✉email: Tayhas_Palmore@brown.edu

Combustion of fossil fuels is the leading cause of global warming due to the accumulation of CO₂ in the atmosphere^{1,2}. The electrochemical CO₂ reduction reaction (CO₂RR), driven by renewable energy, is a promising strategy to reduce CO₂ accumulation. By converting CO₂ into products of higher value, a closed-loop carbon economy begins to emerge^{3–7}. To make CO₂RR economically viable, efficient electrocatalysts with high selectivity for targeted products at scale are needed. Among the metals studied, copper is the only metal known for its intrinsic ability to convert CO₂ into hydrocarbons and alcohols via electrochemical CO₂RR^{3,8}. Recent progress at improving the performance of Cu-based electrocatalysts for CO₂RR has been demonstrated with porous Cu foams⁹, Cu nanoparticle ensembles¹⁰, oxide-derived Cu¹¹, plasma-treated Cu^{12,13}, Cu nanocubes^{13–15}, Cu nanowires^{16–18}, wet-oxidation processed CuCl-derived Cu¹⁹, and single-crystal Cu^{20,21}.

Despite this progress, further advances are needed for producing electrocatalysts at scale that efficiently convert CO₂ into multi-carbon products. As such, the design of catalysts that selectively produce C₂₊ products via electrochemical CO₂RR should focus on minimizing two competing reaction pathways: (1) the hydrogen evolution reaction (HER) and (2) C₁ product formation (e.g., CH₄, HCOOH). Both pathways reduce the faradaic efficiency (FE) of C₂₊ products by consuming electrons and protons. Moreover, C₁ production reduces the amount of adsorbed carbon intermediates available for surface C–C coupling reactions.

To minimize HER, the first step of electrochemical CO₂RR must be enhanced. This first step involves a one electron, one proton reduction of CO₂ to form adsorbed COOH (*COOH) and is a reaction that is affected by the concentration ratio of dissolved CO₂ to protons ($[CO_2]/[H^+]$) near the electrode surface. The relative concentration of dissolved CO₂ and protons near the electrode surface under conditions used for the electrochemical CO₂RR has been simulated by Gupta et al. and found to be significantly different from bulk concentrations²². In addition, Raciti et al. showed that high current densities observed at highly roughened electrocatalysts cause the pH to increase rapidly¹⁷. Despite the low concentration of protons at high pH, the efficiency of electrochemical CO₂RR is reduced by the limited availability of dissolved CO₂ on a rough electrode surface. Therefore, to favor electrochemical CO₂RR over HER, a catalyst with minimal roughness should be used to mitigate a rise in local pH.

To minimize C₁ product formation, insights gained from simulations of electrochemical CO₂RR should guide catalyst design^{23–27}. These simulations provide an energy landscape that relates the energetics of competing reactions on Cu. For example, the onset potential to form adsorbed CO (*CO) is predicted to be lowest on Cu (211) among the Cu facets simulated: (111), (100), and (211)²⁵. Sandberg et al. showed that once *CO forms on a Cu surface, the barrier to forming the C–C coupling product, *OCCO, is lowest on Cu (100) relative to (111) and (211). In addition, the barrier for CO dimerization decreases with increasing *CO coverage²⁷. Moreover, C₂ product formation follows second-order kinetics with a rate proportional to the concentration of reactive C₁ intermediates such as *CO. Here, the rate determining step is dimerization of *CO to form C₂ products^{28–30}. Other unsaturated C₁ intermediates derived by reduction of *CO (i.e., *CHO, *COH, *CH₂, and *CHOH) react with *CO to yield C₂₊ products^{23,24,26,31,32}. Thus, high surface coverage of reactive C₁ intermediates is essential and only obtained by a high density of surface defects. Defect sites such as grain boundaries, step sites, and vacancies that result in under-coordinated atoms on the surface of Cu are known to promote C–C coupling^{33,34}. In addition, Cu⁺ and subsurface oxygen are proposed to promote the adsorption of CO₂ and C–C

coupling^{12,35–38}, although the stability of subsurface oxygen remains controversial^{34,35,39,40}.

To maximize the amount of Cu (100) surface, Chen et al. reported cubic microstructures of Cu formed when a Cu foil was cycled between oxidizing and reducing potentials in 0.1 M KCl⁴¹. Other researchers employed a similar method to prepare Cu catalysts with cubic microstructure and studied product selectivity as a function of plasma-treatment¹³, other halide ions⁴², or stability of residual oxides (indicated by ¹⁸O labeling)³⁴. In all cases, the catalysts were more selective for ethylene than methane. However, the FE for C₂H₄ reported in these studies ranged between 15 and 45%. This difference is likely due to the chemical complexity of the electrochemical cycling method employed. In our hands, the electrochemical cycling method used in previous studies produces only cubic microstructures at oxidizing potentials (Supplementary Fig. 1).

Advances made in the previous studies inspired us to study each parameter influencing catalyst performance separately (i.e., chemical species present and their reactivity/solubility, applied potential, pH, and roughness) in order to develop a novel electrochemical method that utilizes these parameters to produce a Cu electrocatalyst selective for C₂₊ products. In this study, electrocatalysts with a balance of high density of defect sites (i.e., under-coordinated Cu) and low roughness are shown to efficiently convert CO₂ to C₂ and C₃ products (FE_{C₂₊} of 72%) via electrochemical CO₂RR. The electrochemical method used to produce these electrocatalysts consists of three steps: (i) anodic halogenation of Cu foils, (ii) subsequent oxide formation in a KHCO₃ electrolyte, and (iii) electroreduction (Fig. 1). Here, chlorinated Cu, brominated Cu, or iodinated Cu were prepared by applying an oxidative potential to Cu foils immersed in 0.1 M KCl, KBr, or KI, respectively, and are henceforth denoted as Cu_KCl, Cu_KBr, and Cu_KI to reflect the different electrolytes used for anodic halogenation. Grazing-Incidence X-ray diffraction (GI-XRD) confirms the presence of Cu(I) halide on the surface of the halogenated Cu foils. Analysis of the morphological and chemical changes by SEM and EDS elucidated the processes by which subsequent surface reconstruction occurs. EDS also provides evidence that subsurface oxygen at the defect sites of Cu_KCl, Cu_KBr, and Cu_KI are produced via oxidation of Cu by high local pH of the electrolyte. The performance of these electrocatalysts provides strong evidence that both a high density of defect sites and low roughness are critical to promoting the formation of C₂₊ products via electrochemical CO₂RR by minimizing competing HER and C₁ production.

Results

Preparation of electrocatalysts. Halogenated Cu foils were prepared by applying an oxidative potential to electropolished Cu foils immersed in an electrolyte containing halide ions. A three-electrode configuration was used: Cu-foil working electrode, Pt gauze counter electrode, and Ag/AgCl reference electrode. The open circuit potential (OCP) of Cu foil immersed in 0.1 M KCl, KBr, or KI aqueous electrolyte was -0.115 , -0.134 , and -0.315 V vs. Ag/AgCl, respectively (see Supplementary Fig. 2). Chronoamperometric potentials of 1.1, 0.18, and -0.2 V vs. Ag/AgCl were applied to a Cu-foil working electrode while immersed in 0.1 M KCl, KBr, or KI, respectively. Note that the working electrode experiences an effective potential (V_{eff}) defined as $V_{\text{eff}} = V_{\text{app}} - V_{\text{oc}}$, where V_{app} is the applied potential and V_{oc} is the measured OCP. For example, an applied potential of -0.2 V vs. Ag/AgCl in 0.1 M KI corresponds to an effective potential of 0.115 V vs. Ag/AgCl, which anodically iodates the Cu. Current density vs. anodic halogenation time for each electrolyte is shown in Supplementary Fig. 2.

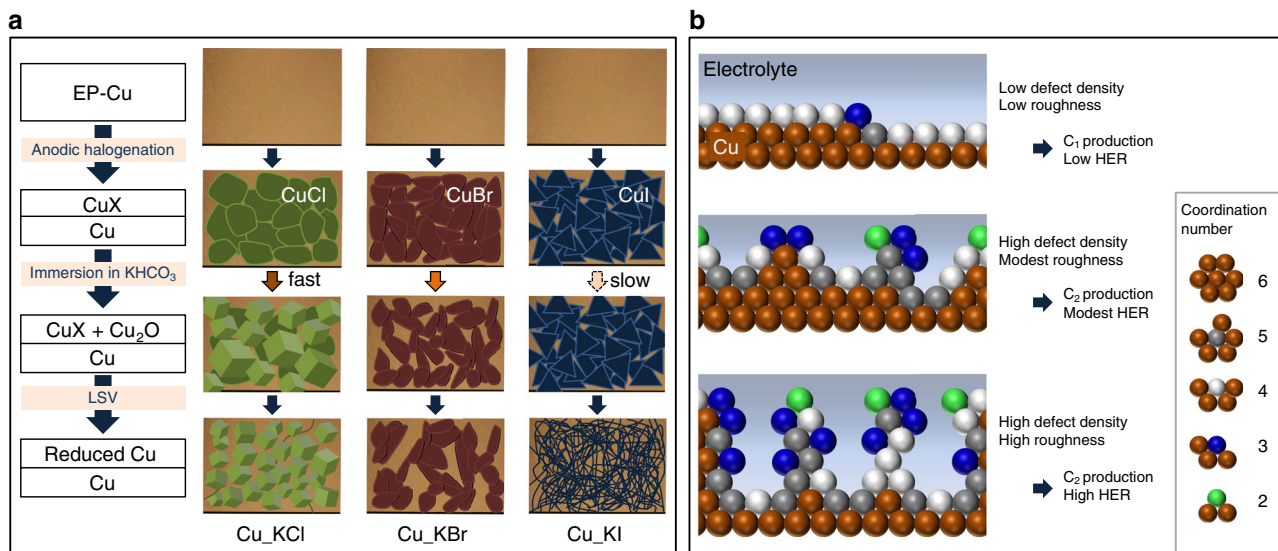


Fig. 1 Schematics showing morphology of Cu catalysts. **a** The method used to prepare Cu catalysts for electrochemical CO₂RR: anodic halogenation in KX solutions where X = halogen, oxide formation in basic KHCO₃, and electroreduction in neutral KHCO₃ by LSV. EP-Cu corresponds to electropolished Cu foils, LSV corresponds to linear sweep voltammetry. **b** Two-dimensional visualization of under-coordinated Cu atoms and surface roughness with the corresponding outcomes when used for the electrochemical CO₂RR. This schematic is simplified but face-centered cubic Cu has a coordination number of 12.

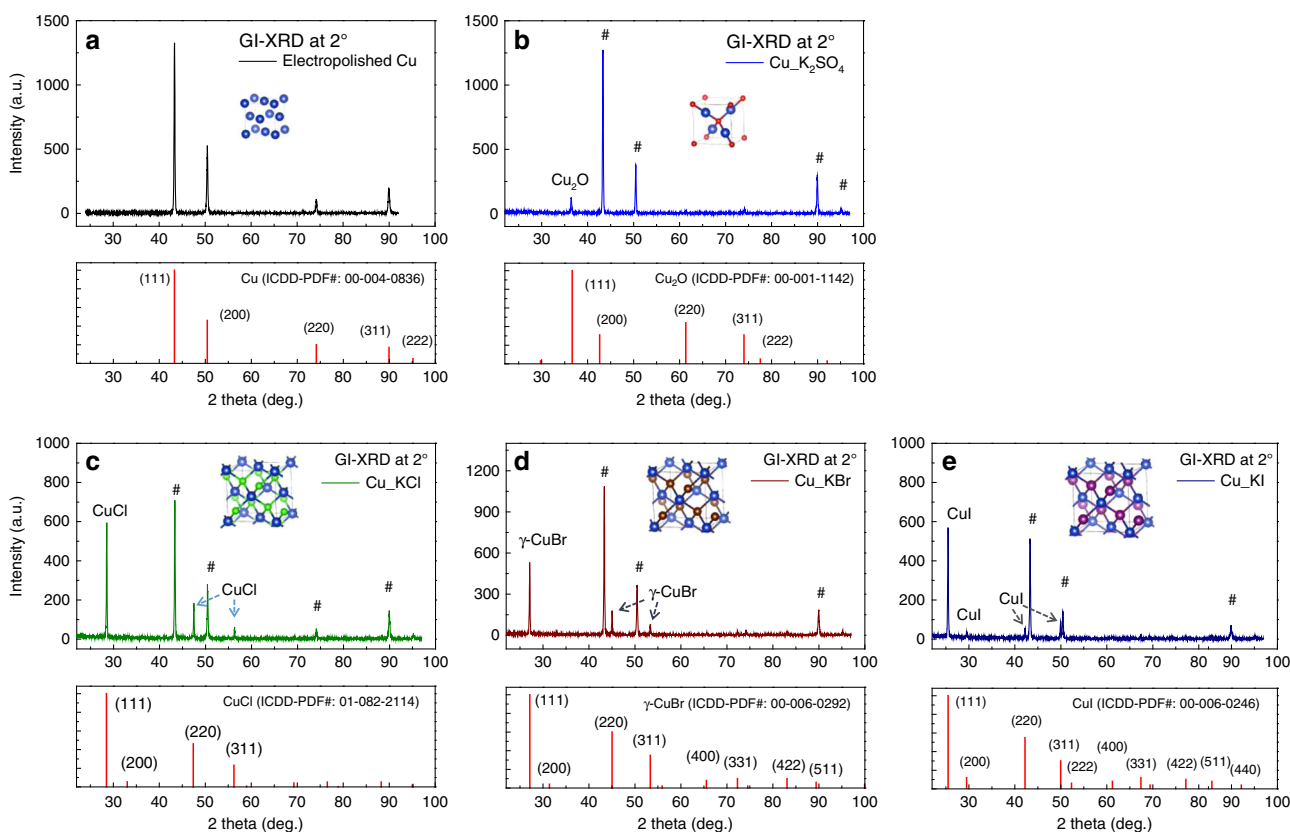


Fig. 2 Crystal structures of halogenated Cu identified by grazing incident X-ray diffraction. GI-XRD patterns of the original electropolished Cu foil (**a**). Cu foils oxidized in 0.05 M K₂SO₄ at 1.1 V vs. Ag/AgCl for 300 s (control sample) (**b**), or halogenated in KCl (**c**), in KBr (**d**), and in KI (**e**) for 100, 60, and 30 s, respectively. The symbol # indicates peaks corresponding to the underlying Cu-foil substrate. The incidence angle used for GI-XRD was 2°. The inset of each GI-XRD plot is a diagram of the unit cell for Cu, Cu₂O, CuCl, CuBr, and CuI, from (**a**) to (**e**), respectively. Cu atoms are represented as blue spheres. Source data are provided as a Source data file.

Evaluation of changes in the crystal structure of Cu_KX. The crystal structure of Cu foils subjected to anodic halogenation was identified by grazing incident X-ray diffraction (GI-XRD) (Fig. 2). Included in this figure is GI-XRD data of control samples: the

original electropolished Cu foil (Fig. 2a) and of electropolished Cu foil after being oxidized in the absence of halide ions (0.05 M K₂SO₄ aqueous electrolyte, 1.1 V vs. Ag/AgCl, 300 s) (Fig. 2b). The GI-XRD data of the control sample shows that oxidation in

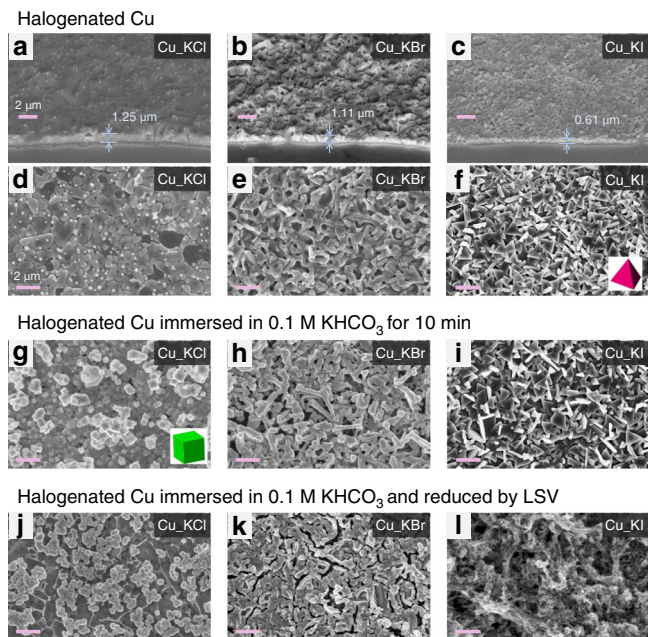


Fig. 3 Morphology of halogenated Cu-foil electrodes. SEM images of halogenated Cu foils: **a–f** as-prepared; **g–i** after immersion in 0.1 M KHCO_3 for 10 min; **j–l** after reduction by LSV in the potential range from OCP to -1.8 V in CO_2 -saturated 0.1 M KHCO_3 . **a–c** Cross-sectional images taken at a tilt angle of 45° to reveal the thickness of halogenated Cu. **d–f** Plan-view images. Anodic halogenation of Cu was performed for 50 s in 0.1 M KCl at 1.1 V (**a, d, g, j**); in 0.1 M KBr at 0.18 V (**b, e, h, k**); in 0.1 M KI at -0.2 V (**c, f, i, l**). All voltages are reported vs. Ag/AgCl. Scale bars: 2 μm .

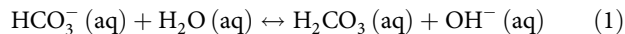
the absence of halide ions produces Cu_2O on the surface of the Cu foil. In contrast, anodic halogenation of electropolished Cu foils in KCl, KBr, or KI results in the formation of CuCl, CuBr, or CuI, respectively (Fig. 2c–e).

Evaluation of changes in the morphology of Cu_KX. The morphology of the Cu foils was expected to change with changes in crystal structure. Therefore, SEM was used to examine samples subjected to anodic halogenation for 50 s (Fig. 3). SEM images of samples halogenated for other lengths of time and at different applied potentials are shown in Supplementary Figs. 3–7 and SEM images of the control sample are shown in Supplementary Fig. 8. Cross-sectional images of the samples reveal that a halogenated Cu layer forms on electropolished Cu foils during anodic halogenation in KCl, KBr, or KI for 50 s to a thickness of 1.25, 1.11, and 0.61 μm , respectively (Fig. 3a–c). Plan-view SEM images of the as-prepared Cu(I) halide are shown in Fig. 3d–f. The formation of a surface layer of Cu(I) halide during anodic halogenation causes a volume expansion that results in surface wrinkling to relieve mechanical stress. This wrinkling is observed in Cu_KCl and Cu_KBr samples but not in the Cu_KI sample, where instead, triangle-based pyramids emerge.

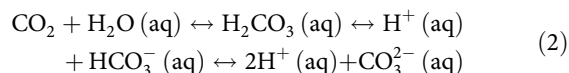
The catalysts were subjected to two additional treatments to determine if the morphology of the surface changes further when halogenated Cu foils are immersed in an electrolyte commonly used for CO_2RR experiments: (1) immersion in air-saturated KHCO_3 , where the pH is basic and (2) electrochemical reduction in CO_2 -saturated KHCO_3 , where the pH is nearly neutral (pH 6.8). These two experiments model the environment that catalysts encounter in preparation for the CO_2RR but separate the effect of basic pH from that of reducing potentials at near neutral pH.

For the first experiment, all Cu_KX samples (where X is a halogen) were immersed in air-saturated 0.1 M KHCO_3 for 10

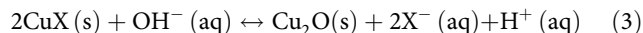
min. An air-saturated solution of 0.1 M KHCO_3 has a measured pH of 9.0, whose basicity is derived from a shift in equilibrium from bicarbonate ion to its weak acid (H_2CO_3) to produce OH^- ions:



When purged with CO_2 (as in the case for the CO_2RR), the KHCO_3 electrolyte becomes more acidic (pH 6.8) because of the formation of carbonic acid:

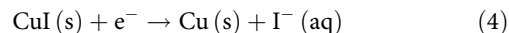


Based on calculated equilibrium diagrams, Cu_2O is more stable than CuCl at pH 9 and OCP^{43,44}. Thus, any morphological changes that may occur when Cu_KX is immersed in KHCO_3 will be caused by an oxide-forming reaction that converts the Cu(I) halide into Cu_2O :



In addition, morphological changes should reflect the coordination affinity of copper(I) halides ($\text{CuCl} < \text{CuBr} < \text{CuI}$)^{45,46} and their solubility product (K_{sp}) in aqueous solution ($\text{CuCl} > \text{CuBr} > \text{CuI}$)⁴². Consequently, when Cu_KCl is immersed in an air-saturated solution of 0.1 M KHCO_3 (pH 9.0) for 10 min, the relatively unstable CuCl is converted rapidly to Cu_2O with cubic morphology (Fig. 3g). The cubic morphology reflects the relative growth kinetics of different facets, where the direction of slowest growth corresponds to the largest facet⁴⁷. Thus, the emergence of cubic morphology during the conversion of CuCl to Cu_2O suggests that the chloride ions released during this reaction adsorb preferentially on the (100) facet, impeding its growth kinetics. This observation is consistent with simulations that have shown the preferential adsorption of halide ions onto the (100) facet of Cu⁴⁸. When Cu_KBr is subjected to the same treatment, the wrinkled surface of CuBr appears only to shrink slightly from the release of bromide ions into the electrolyte during the oxide-forming reaction [Eq. (3)] (Fig. 3h). In contrast, when Cu_KI is subjected to the same treatment, the highly stable and insoluble CuI does not undergo any significant morphological change (Fig. 3i). GI-XRD data further supports the effect of halide ion on the extent to which CuX is converted into Cu_2O in basic KHCO_3 (see Supplementary Fig. 9). These observations are consistent with the trend in stability and solubility of Cu(I) halides and correspond to different rates of oxide formation via [Eq. (3)].

For the second experiment, all Cu foils that had been anodically halogenated and converted to oxide in air-saturated KHCO_3 were reduced by LSV from the measured OCP to -1.8 V vs. Ag/AgCl at a scan rate of 5 mV/s (Supplementary Fig. 10). The resulting GI-XRD data (Supplementary Fig. 11) is nearly identical to that of the original electropolished Cu, indicating electroreduction by LSV extracts halide ions from the Cu_KX samples. Consequently, reduction of Cu_KCl results in a morphology with smaller but more uniformly sized cubic structures than before (Fig. 3j) and reduction of Cu_KBr results in further shrinkage and consequential formation of cracks (Fig. 3k). The reduction of Cu_KI results in a dramatic change to its morphology (Fig. 3l) and is attributed to the rapid reduction of iodinated Cu:



Recall, Cu_KI does not undergo significant oxide formation in the prior experiment (i.e., immersion in air-saturated KHCO_3 electrolyte). Thus, the electrochemical reduction of Cu_KI causes an abrupt release of iodide ions, leading to the dramatic change in morphology that is observed. In contrast, bromide ions from Cu_KBr are released gradually by the oxide-forming reaction

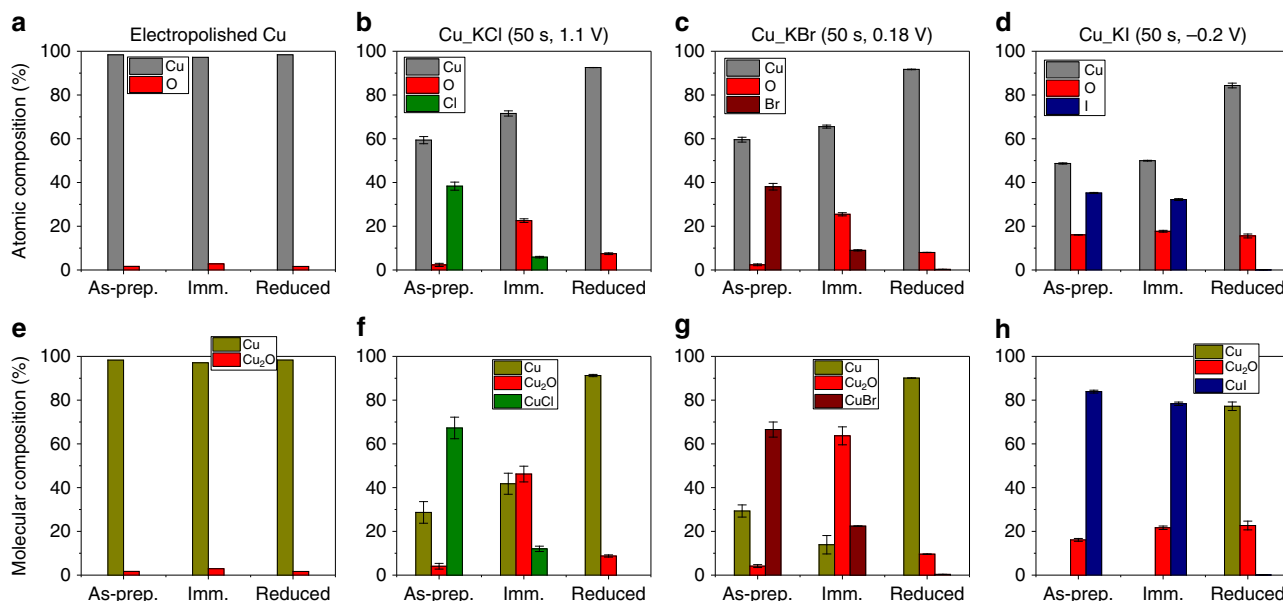


Fig. 4 Energy-dispersive X-ray spectroscopy. **a–d** Raw data of atomic composition of electropolished Cu foil and halogenated Cu foils as measured by EDS. **e–h** Compositions of molecular species from converted EDS data. ‘As-prep.’ indicates the as-prepared catalyst by electropolishing or anodic halogenation. ‘Imm.’ indicates the catalyst underwent oxide formation by immersion in air-saturated 0.1 M KHCO_3 electrolyte for 10 min. ‘Reduced’ indicates the catalyst was reduced in CO_2 -saturated 0.1 M KHCO_3 electrolyte by LSV from its corresponding OCP to -1.8 V vs Ag/AgCl at a scan rate of 5 mV/s. Source data are provided as a Source data file.

before the sample is subjected to electrochemical reduction. Cu_2KCl undergoes relatively rapid oxide formation in KHCO_3 electrolyte so that its morphology has already changed prior to being subjected to electrochemical reduction.

Evaluation of changes in the chemical composition of Cu_2KX .

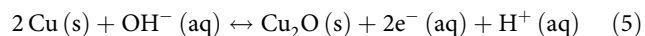
The elemental compositions (Cu, O, and halogen atoms) of the surface of Cu_2KX were determined using EDS for the purpose of relating changes in chemical composition to changes in morphology. Raw EDS data are shown in Fig. 4a–d, which can be converted into compositions of molecular species (Fig. 4e–h) using the chemical species identified by GI-XRD experiments. Details on the conversion of EDS data into chemical species can be found in the Supplementary Information. It is assumed that the halogenated catalysts consist of only three chemical species (i.e., Cu, Cu_2O , and CuX) because other species such as CuO were not observed in the GI-XRD data (see Supplementary Figs. 9 and 11). In the case of electropolished Cu, only two chemical species are assumed to exist: Cu and Cu_2O .

The initial surface species of Cu_2KCl and Cu_2KBr are converted into Cu_2O by the oxide-forming reaction [Eq. (3)] when the samples are immersed in air-saturated 0.1 M KHCO_3 for 10 min (Fig. 4f, g). For example, EDS data indicates the as-prepared Cu_2KCl contains 4.06% of Cu_2O and 67.3% of CuCl . Similarly, as-prepared Cu_2KBr contains 4.13% of Cu_2O and 66.6% of CuBr . After immersion, rapid oxide formation occurs: Cu_2KCl contains 46.2% of Cu_2O and 12.0% of CuCl while Cu_2KBr contains 63.7% of Cu_2O and 22.4% of CuBr . Unlike Cu_2KCl and Cu_2KBr samples, Cu_2KI showed only slight changes to the composition of the initial surface species due to the high stability of CuI in basic KHCO_3 . The as-prepared sample contained 16.1% of Cu_2O and 83.9% of CuI whereas the immersed sample contained 21.6% of Cu_2O and 78.3% of CuI (Fig. 4h).

Electrochemical reduction of Cu_2KX samples by LSV is expected to reduce all Cu(I) species to Cu^0 . The converted EDS data reveal (Fig. 4g, h), however, that 0.33% of CuBr and 0.12% of

CuI remains on the surface of the respective catalysts with the Cu_2KI sample having a relatively higher content of Cu_2O (22.7%) than either the Cu_2KCl or Cu_2KBr samples (<10%). More detailed analysis of residual halide using XPS and EDS are shown in Supplementary Figs. 12 and 13. After electrochemical reduction, the high content of Cu_2O in the Cu_2KI is likely due to re-oxidation of the surface upon exposure to air during the time between sample preparation and EDS measurement (<30 min) and indicates that reduced Cu_2KI is particularly susceptible to re-oxidation by air. This conclusion is consistent with the fact that Cu_2KI undergoes abrupt morphological and chemical changes when electrochemically reduced by LSV, which generates a high density of under-coordinated atoms on the surface of the catalyst. Furthermore, this conclusion is supported by the work of Lum et al., where oxide-derived (OD) Cu with a high density of grain boundaries, could be re-oxidized very quickly when exposed to ambient air and moisture³⁴.

The chemical composition of electropolished Cu does not change significantly when immersed in air-saturated KHCO_3 for 10 min and subsequently electrochemically reduced by LSV as shown in the converted EDS data (Fig. 4e). The percentage of Cu_2O at electropolished Cu, however, does increase slightly from 1.7 to 2.9% upon immersion in air-saturated KHCO_3 for 10 min. This slight increase in Cu_2O occurs via the oxidation reaction predicted by the Pourbaix diagram for copper^{22,49}:



As such, this reaction is likely to be a weak but important driving force that enables electrocatalysts to maintain a small amount of Cu^+ and subsurface oxygen despite the highly negative potentials used for electrochemical CO_2RR . The mechanism by which Cu^+ species are stable to conditions used for CO_2RR , however, remains indeterminate¹². Nevertheless, because basic pH favors the oxidation reaction that forms Cu_2O [Eq. (5)] (i.e., hydroxide ions are consumed and protons are released), the rate of this reaction is enhanced during the electrochemical CO_2RR , where protons are consumed and the pH near the electrode increases

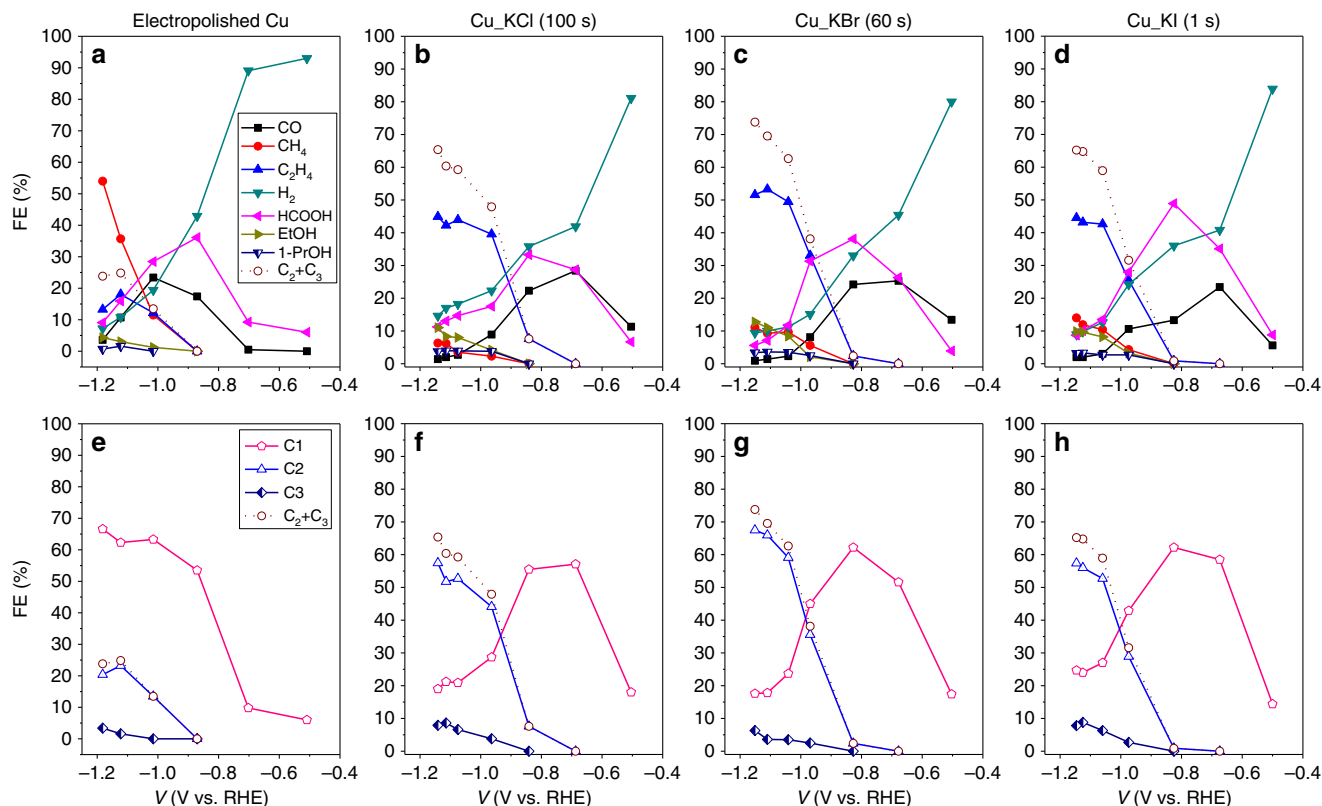


Fig. 5 Performance of catalysts for electrochemical CO₂ reduction reaction. Potential-dependent faradaic efficiency of the products from the CO₂RR products on electropolished Cu (**a**), chlorinated Cu (**b**), brominated Cu (**c**), and iodinated Cu (**d**). Anodic halogenation of Cu was performed in 0.1 M KCl at 1.1 V vs. Ag/AgCl for 100 s (**b**); in 0.1 M KBr at 0.18 V vs. Ag/AgCl for 60 s (**c**); in 0.1 M KI at -0.2 V vs. Ag/AgCl for 1 s (**d**). **e–h** FEs of C₁, C₂, and C₃ products from the same results shown in the corresponding upper plot. C₁ products include CO, formate, and CH₄. C₂ products include C₂H₄, ethanol, acetate, acetaldehyde, and glycolaldehyde. C₃ products include n-propanol, propionaldehyde, and allyl alcohol. Data were acquired during 40 min of electrochemical CO₂RR at a constant potential in 0.1 M KHCO₃ saturated with CO₂. FE is shown as a function of the *i*R-corrected potential in RHE scale. Data legends apply to all plots in the same row. Source data are provided as a Source data file.

significantly. Thus, when a catalyst has defect sites that are susceptible to re-oxidation (e.g., oxide-derived Cu¹¹ or plasma-activated Cu¹²), the oxidation reaction [Eq. (5)] will generate C⁺ and subsurface oxygen at those defect sites where the local pH is high during the electrochemical CO₂RR. Notably, Lum et al. found that oxygen species of oxide-derived Cu are unstable and reduced at the highly negative potential, however, the rapid re-oxidation of Cu possessing a high density of defect sites occurs merely by soaking in 0.1 aqueous KHCO₃ electrolyte³⁴. Their observation is consistent with Eq. (5) that basic pH of the electrolyte oxidizes Cu.

Evaluating catalyst performance for electrochemical CO₂RR.

To test the activity and selectivity of the halogenated Cu catalysts, bulk electrolysis of CO₂ was performed at a constant potential in CO₂-saturated 0.1 M KHCO₃ for 40 min. Electrochemical CO₂RR experiments were performed over a potential range from -1.1 to -2.1 V vs. Ag/AgCl (with *i*R-compensation these potentials correspond to -1.1 to -1.78 V vs. Ag/AgCl or -0.50 to -1.18 V vs. RHE). The resulting potential-dependent FEs from these experiments are shown in Fig. 5. The catalysts were prepared via anodic halogenation of a Cu foil for different lengths of time (i.e., 100 s for Cu_KCl, 60 s for Cu_KBr, and 1 s for Cu_KI) to ensure complete coverage of the Cu substrate with Cu(I) halide (see Supplementary Figs. 4–6). The major product obtained on Cu(I)-halide-derived catalysts was C₂H₄, with its highest FE (45.1% on Cu_KCl, 49.5% on Cu_KBr, and 44.5% on Cu_KI) observed at ~ -1.15 V vs. RHE (see Table 1). For comparison, the major

product obtained on electropolished Cu was CH₄, with its highest FE (54.0%) at the same potential. Moreover, the Cu(I)-halide-derived catalysts produced CO with FEs in the range of 23–28% at potentials as low as ~ -0.68 V vs. RHE whereas electropolished Cu at this potential yielded CO with a FE of only 0.5%. Adsorbed CO (*CO) is an important intermediate required for production of C₂ and C₃ products via C–C bond coupling. The rate of reaction to produce C₂H₄ is second order with respect to the surface concentration of adsorbed CO (*CO). Thus, a high density of active sites on the surface of the catalyst is necessary to produce a high surface concentration of *CO.

The effect of anodic halogenation time on CO₂RR performance also was investigated (Fig. 6). All data shown in Fig. 6 were collected at -1.11 V vs. RHE, where the FE for H₂ was the lowest amongst all applied potentials studied. Supplementary Figs. 4–6 reveals that the underlying electropolished Cu substrate is exposed when anodic halogenation is performed for short periods of time. Thus, the Cu_KX catalysts produced by anodic halogenation for a short reaction time showed relatively high amounts of CH₄ and low amounts of C₂H₄ and H₂, a product distribution expected from electropolished Cu. Thus, to completely cover the underlying Cu substrate by Cu(I) halide, anodic halogenation needs to be applied for at least 60 s for Cu_KCl, 60 s for Cu_KBr and 5 s for Cu_KI. For these reaction times, 3.82, 0.80, and 0.028 C cm⁻² of charge per unit area of electrode was used to make CuCl, CuBr, and CuI layers on electropolished Cu, respectively. The amount of charge vs. different amounts of time used for anodic halogenation is shown in Supplementary Fig. 14.

Table 1 Representative FEs of products from electrochemical CO₂RR shown in Figs. 5 and 6.

Catalyst	V _{appl} (Ag/AgCl)	J (mA/cm ²)	V _{comp} (Ag/AgCl)	V _{comp} (RHE)	FE (%)													
					CO	CH ₄	C ₂ H ₄	H ₂	HCOO ⁻	EtOH	PrOH	Other	Total	C ₁	C ₂	C ₃	C ₂₊	
Fig. 5	EP-Cu	19.6	-1.78	-1.18	3.6	54	13.28	7.2	9.1	4.4	0.7	5.5	97.6	66.6	20.4	3.4	23.82	
	Cu ₂ KCl	45.5	-1.73	-1.14	1.7	5.8	45.14	14.6	11.2	11	3.7	5.7	98.9	18.7	57.7	7.9	65.60	
	100 s																	
	Cu ₂ KBr	42.7	-1.75	-1.15	1.0	9.6	49.47	11.7	5.6	12.8	3.4	6.1	98.2	16.2	65.4	6.3	71.71	
	60 s																	
Fig. 6	Cu ₂ KI	40.0	-1.74	-1.15	2.0	14	44.54	8.9	8.7	9.8	3.2	7.7	98.8	24.7	57.4	7.8	65.21	
	1 s																	
	Cu ₂ KCl	40.3	-1.71	-1.11	1.6	4.1	50.15	12.0	9.7	10.9	4.3	5.3	98.1	15.4	62.9	7.9	70.73	
	60 s																	
	Cu ₂ KBr	43.3	-1.70	-1.10	2.3	1.7	50.94	13.8	8.7	12	4.4	4.2	98.0	12.6	64.4	7.2	71.54	
90 s																		
Cu ₂ KI	40.0	-1.69	-1.09	1.5	8.4	49.99	9.3	9.2	13.8	5.2	3.6	98.0	19.1	65.3	7.2	72.58		
10 s																		

A relatively short amount of time of anodic halogenation covers the Cu substrate with CuI because iodide ions have a high ligand affinity for Cu^{45,46} and the resulting CuI is highly stable⁴². In contrast, anodic chlorination or bromination of Cu requires more time to completely cover the Cu surface.

When the halogenation reaction time is increased up to 300 s, the FE for H₂ on all three Cu(I)-halide-derived catalysts increases significantly (i.e., FE for H₂ was 17.4% on Cu_KCl, 15.1% on Cu_KBr, and 19.9% on Cu_KI). To minimize the competing HER reaction, an optimal halogenation time was sought for each Cu_KX catalyst. The Cu_KCl catalyst that generated C₂H₄ with a FE of 50.2% and C₂₊ products with a FE of 70.7% was prepared using an anodic chlorination time of 60 s. Likewise, the Cu_KBr catalyst that generated C₂H₄ with a FE of 50.9% and C₂₊ products with a FE of 71.5% was prepared using an anodic bromination time of 90 s and the Cu_KI catalyst that generated C₂H₄ with a 50.0% and C₂₊ products with a FE of 72.6% was prepared using an anodic iodination time of only 10 s (see Table 1).

Roughness factor, local pH, and competing HER. Anodic halogenation generates a high density of active sites, which can be crystal grain boundaries or defect sites such as step atoms or under-coordinated atoms. These active sites in turn increase the production of C₂ products from CO₂RR. If halogenation time is too long, however, the competing HER increases because the surface of the catalyst becomes too rough (see Supplementary Scheme 1). The roughness factor of an electrocatalyst can be determined by the double-layer (DL) capacitance method with the assumption that the surface charge is constant across different kinds of catalysts (see Supplementary Fig. 15). Figure 7a shows the relative roughness of Cu_KX as measured by DL capacitance, which are related as:

$$\text{roughness factor} = \frac{\text{DL capacitance of the catalyst}}{\text{DL capacitance of the electropolished Cu}}$$

Higher surface roughness promotes more HER. Figure 7a shows the relationship between the roughness of the catalysts, FE for H₂, and halogenation time. This correlation between roughness and HER can be explained by a decrease in the concentration ratio of dissolved CO₂ to proton ([CO₂]/[H⁺]) near the surface of the catalyst at high local pH. Although the buffering capacity of the bicarbonate electrolyte minimizes any increase in pH, the high current density observed at catalysts with high roughness rapidly depletes protons in the interfacial region and leads to a high local pH^{17,22}. With high local pH, dissolved CO₂ becomes bicarbonate and carbonate ions by the equilibrium reaction shown in Eq. (2). The concentrations of dissolved CO₂, bicarbonate and carbonate ions, and protons in the electrolyte were calculated and are shown in Fig. 7b (details on this calculation are given in Supplementary Information and shown in Supplementary Fig. 16). The normalized concentration ratio of [CO₂]/[H⁺] (and its inverse) is shown in Fig. 7c, which at pH 6.8 and 9.9 is 0.706. In contrast, the maximum concentration ratio of [CO₂]/[H⁺] occurs at pH 8.3. Above pH 9.9, the concentration ratio of [CO₂]/[H⁺] decreases rapidly so that HER is favored over electrochemical CO₂RR. In other words, a catalyst with higher roughness produces a higher current density in electrochemical CO₂RR. A high current density rapidly consumes reactants, which are dissolved CO₂ and protons in the interfacial region between the catalyst and the electrolyte. The rapid consumption of protons results in a rise in the local pH. A high local pH decreases the concentration ratio of dissolved CO₂ to proton ([CO₂]/[H⁺]) at the interfacial region by the equilibrium reaction [Eq. (2)]. Consequently, a lower [CO₂]/[H⁺] at a pH above 9.9 favors the competing HER side reaction. Data taken from the literature and included in Supplementary

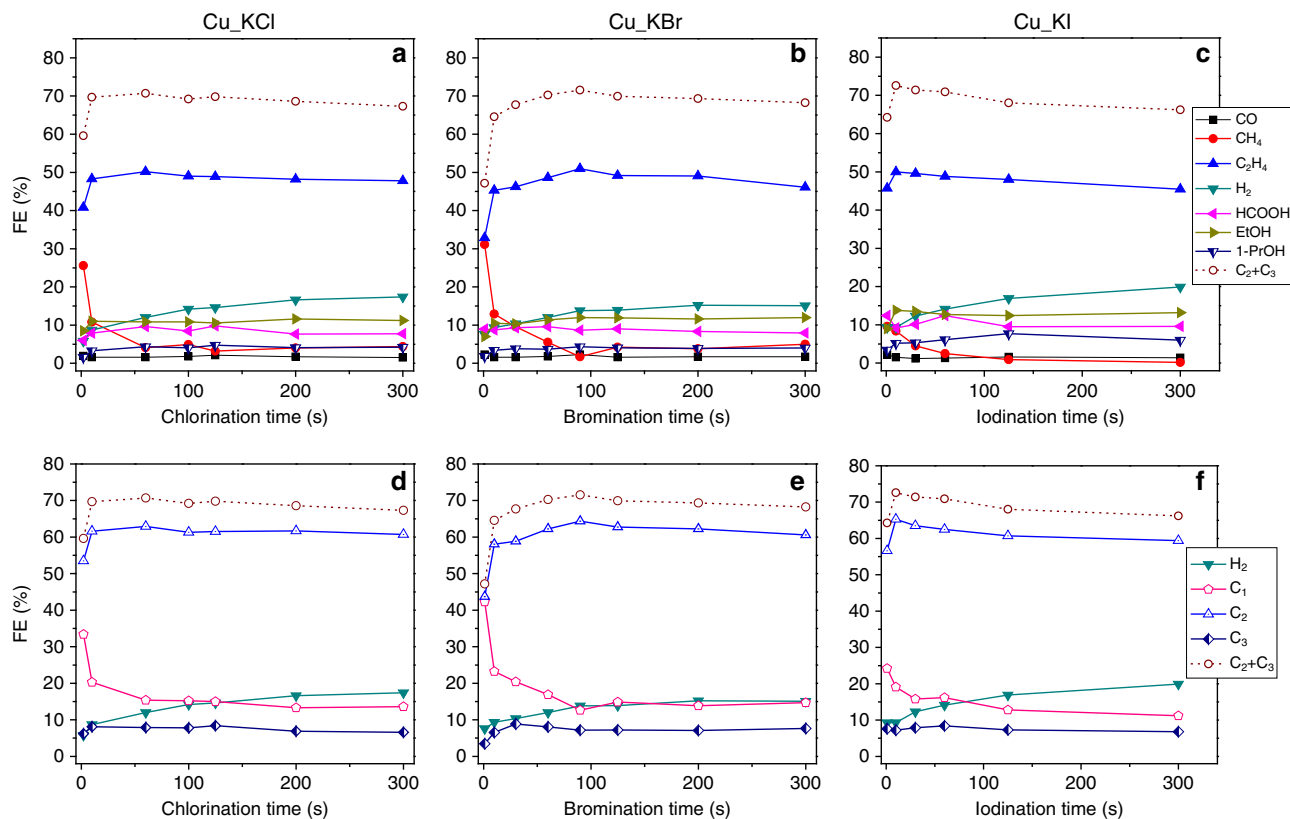


Fig. 6 Effect of halogenation time on the performance of the catalysts for CO_2 reduction reaction. FEs of the products from electrochemical CO_2 RR are shown versus the amount of time the Cu foils were subjected to anodic halogenation in KCl (**a**), KBr (**b**), and KI (**c**). **d-f** FEs of H_2 , C_1 , C_2 , and C_3 products from the same results shown in the corresponding upper plot. Data were acquired during 40 min of electrochemical CO_2 RR at a constant potential of -1.11V vs. RHE in 0.1M KHCO_3 saturated with CO_2 . Data legends apply to all plots in the same row. Source data are provided as a Source data file.

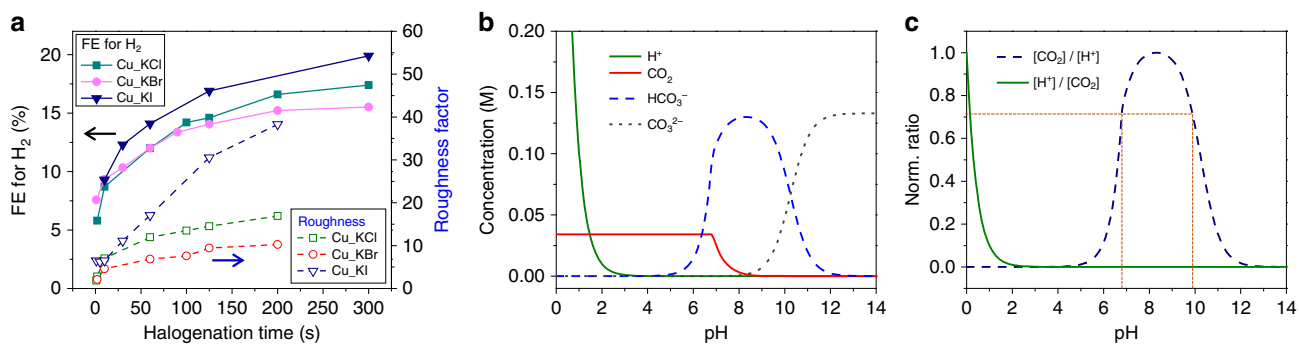


Fig. 7 Relation between surface roughness of the electrocatalysts and HER. **a** The roughness factor of the catalyst was estimated from the double-layer capacitance as measured by cyclic voltammetry (CV) in the potential range from -0.35 to -0.5V vs. Ag/AgCl . FE for H_2 from Fig. 6. **b** Calculated concentrations of reactants and buffering ions in 0.1M KHCO_3 saturated with CO_2 . **c** The normalized concentration ratio of dissolved CO_2 to proton as calculated from Fig. 7b. Source data are provided as a Source data file.

Fig. 17 also reveals a strong correlation between the roughness of the catalyst and the amount of HER. Our observation that mitigation of the rise of local pH suppresses HER is consistent with the previous report by Singh et al.⁵⁰

Discussion

Hori et al. studied single-crystal Cu with a (911) facet introduced a (111) step for every five (100) basal planes $[5(100) \times (111)]^{20}$. The performance of this facet in the electrochemical CO_2 RR was superb, producing H_2 at a FE of 12.7%, C_2H_4 at a FE of 50.9% and C_{2+} products at a FE of 79.5% at a stir rate of 260 rpm [in comparison to polycrystalline Cu, which in our hands produces H_2 at a FE of 15.1%, C_2H_4 at a FE of 20.4% and C_{2+} products at a

FE of 32.6% with a comparable rate of stirring ($\sim 290\text{rpm}$)]. However, producing single-crystal catalysts at a scale required for carbon utilization is not economically or technically feasible. Thus, a simple and inexpensive alternative to single-crystal Cu is to prepare Cu catalysts via anodic halogenation.

More recent studies have proposed the predominant facet (100) of cubic structures of Cu promotes the conversion of CO_2 into multi-carbon products^{14,19}. Although Cu_KCl exhibits cubic structures on its surface, both Cu_KBr and Cu_KI have irregular microstructures (see Fig. 3). All three Cu_KX catalysts, however, have a high density of defect sites and produce C_{2+} products with FEs up to 70.73% on Cu_KCl, 71.54% on Cu_KBr, and 72.58% on Cu_KI. Thus, in addition to specific crystal facets, a high density

of defect sites (i.e., step sites and low-coordinated Cu atoms) is essential for converting CO₂ into C₂ products via electrochemical CO₂RR at a Cu catalyst. This finding is consistent with the results of Hori et al. that Cu (100) single crystal is not an ideal facet for selective C₂₊ production (FE_{CH₄} = 30.4% and FE_{C₂H₄} = 40.4%)²⁰ and the more recent claim that the presence of oxygen species in surface and subsurface regions of catalysts with nano-cubic morphology are more important for achieving high activity and selectivity for C₂₊ hydrocarbons or alcohols than the presence of Cu(100) facets themselves¹³.

Anodic halogenation of electropolished Cu followed by surface reconstruction from base-induced oxide formation and electro-reduction creates a surface with a high density of defect sites. These sites stabilize species such as Cu⁺ and subsurface oxygen, which are known to promote C₂₊ production during the electrochemical CO₂RR. Evidence of a high density of defect sites on the surface of Cu_KX catalysts is provided by incidence-angle dependent GI-XRD data (Supplementary Fig. 18), which shows decreased crystal ordering at the surface of Cu_KBr during surface reconstruction. Furthermore, EDS data reveals the high susceptibility of these surfaces to re-oxidation. The density of defect sites in oxide-derived Cu has recently been determined using positron annihilation spectroscopy (PAS)³⁵. Based on our results, we conclude that a high density of defect sites is the most important attribute of a Cu catalyst that selectively converts CO₂ into C₂₊ products via the electrochemical CO₂RR.

Interestingly, ethane (C₂H₆) is produced when the roughness factor exceeds 30 (FE_{C₂H₆} = ~1.2% in this work). The mechanistic pathway to produce C₂H₆ has been proposed to be the reaction between adsorbed ethylene (*C₂H₄) and adsorbed hydrogen (*H)⁵¹. Therefore, observation of C₂H₆ indicates high surface concentrations of both *C₂H₄ and *H, which only can be attributed to a high density of defect sites and high roughness, respectively. Thus, production of C₂H₆ indicates that the roughness of the catalyst needs to be lowered to obtain the optimal balance of a high density of defect sites that favors C₂H₄ production and low roughness that suppresses HER.

Recently, Wang et al. reported a wet-chemistry method to prepare cuprous-halide-derived catalysts with FE up to 58% for C₂₊ product⁵². Our study significantly advances this reaction to obtain a FE of 72.6% for C₂₊ product. This advance is made possible by the discovery that features of Cu catalysts can be optimized for this reaction (e.g., defect density, roughness) by controlling the duration of anodic halogenation at a constant potential. Our study also highlights the importance of the correlation between the roughness of the catalyst and HER and the impact of that correlation on electrochemical CO₂RR at negative potentials (~ -1 V vs. RHE). Thus, the [CO₂]/[H⁺] ratio provides an important parameter that can be controlled to yield a catalyst that is both efficient and selective for C₂₊ products.

In summary, Cu(I)-halide-derived catalysts were prepared using anodic halogenation. The optimal time and voltage for anodic halogenation was 60–100 s at 1.1 V, 60–90 s at 0.18 V, and 10 s at -0.2 V vs. Ag/AgCl for Cu_KCl, Cu_KBr, and Cu_KI, respectively. Iodide ions react with the Cu surface rapidly at weak oxidative potentials because of the high affinity of I⁻ to form CuI. All Cu(I)X-derived catalysts (where X = Cl, Br, or I) were found to be excellent catalysts for producing C₂₊ products via the electrochemical CO₂RR with FE_{C₂₊} of 70.7%, 71.5%, and 72.6% on Cu_KCl, Cu_KBr, and Cu_KI, respectively. By exploiting volume changes that occur during anodic halogenation and subsequent surface reconstruction, we show that anodic halogenation is a simple to perform and scalable method for consistently preparing Cu catalysts with a high density of surface defect sites and low roughness. The high density of defect sites promotes production of multi-carbon products and the low

roughness suppresses the competing HER. These results, taken together, provide an approach to preparing catalysts for efficient conversion of CO₂ to C₂₊ products that has characteristics desirable for carbon utilization technologies: simple to perform, consistent, regenerative, and scalable.

Methods

Preparation of electrocatalysts. All Cu foils were mechanically polished with 400 grit sandpaper, and rinsed with deionized (DI) water. The Cu foils (2 × 5 cm²) subsequently were electropolished by chronoamperometry in 85% phosphoric acid at 1.5 V with a Cu counter electrode in a two-electrode configuration. The electropolished Cu foils were rinsed with DI water. After cutting the electropolished Cu foils into 2 × 0.5 cm² pieces, the foils were flattened and both the back side and part of the front side were covered with polyimide (PI) tape to define the geometric area of the working electrode. The electrode was wrapped in PTFE tape (Swagelok) to prevent detachment of the PI tape. The exposed geometric area was typically 0.35 cm². KCl (Macron fine chemicals), KBr (Fisher Scientific), and KI (Fisher Scientific) were dissolved in DI water to a concentration of 0.1 M. Anodic chlorination, bromination, and iodination was performed on an electropolished Cu foil immersed in 0.1 M KCl, KBr, and KI at 1.1, 0.18, and -0.2 V vs. Ag/AgCl, respectively, in a three-electrode configuration using a potentiostat (Pine Instrument Company, Biopotentiostat, model AFCBP1). The counter electrode was Pt gauze and the reference electrode was Ag/AgCl (saturated KCl) electrode. The OCP of electropolished Cu in 0.1 M KCl, KBr, and KI was -0.115, -0.134, and -0.315 V vs. Ag/AgCl, respectively (Supplementary Fig. S1).

Characterization of the electrocatalysts. SEM images were acquired using a LEO 1530 VP ultra-high resolution field emitter SEM at 10 kV. Elemental analysis of samples was obtained using the EDS accessory (Oxford Instruments, Inca X-sight, model 7426) of the SEM. The GI-XRD data were obtained using a Bruker D8 Discovery High resolution X-ray Diffractometer at incidence angle of 2° and wavelength of 1.54 Å. The double-layer capacitance was measured by cyclic voltammetry in the potential range from -0.35 to -0.5 V vs. Ag/AgCl in CO₂-saturated 0.1 M KHCO₃ after electrochemical CO₂RR. XPS equipment of PHI 5000 VersaProbe (Ulvac-PHI, Japan) was used to characterize the surface of the Cu catalysts.

Electrochemical CO₂ reduction. Electrochemical CO₂RR was carried out in a custom made two compartment cell, separated by a Nafion 117 proton-exchange membrane. The two compartments were filled with 8.2 ml of 0.1 M KHCO₃ (Sigma-Aldrich, ≥99.95%) electrolyte. A three-electrode configuration was employed: Cu-foil working electrode, Pt gauze counter electrode, and a home-built Ag/AgCl reference electrode. The working and reference electrodes were placed in the cathode compartment and the Pt gauze counter electrode was placed in the anode compartment. Prior to initiating electrochemical CO₂RR, the halogenated Cu-foil electrode was immersed in 0.1 M KHCO₃ electrolyte and linear sweep voltammetry was performed with a scan rate of 5 mV/s from the OCP to the working potential (usually -0.2 to -2.1 V vs Ag/AgCl). Subsequently, CO₂RR was performed with fresh electrolyte saturated with CO₂. Before and during electrochemical CO₂RR, the cell was purged continuously with CO₂ at a flow rate of 20 mL/min as measured with a rotameter (OMEGA FL-3841G FT-032-41-GL-VN). Electrochemical CO₂RR was performed by chronoamperometry for 40 min with a magnetic stirring bar spinning at ~1500 rpm. A Thermolyne Nuova stir plate (model No. SP18425) was used to stir a 1-cm-long magnetic bar in the electrolyte. The stirring speed was calibrated in comparison with the Fisher Scientific hot plate/stirrer (Cat. No. 11-100-49SH). It is worth noting that all experimental results on electrochemical CO₂RR were obtained while stirring the electrolyte with a magnetic stirrer at ~1500 rpm.

After electrochemical CO₂RR, the solution resistance (*R*) was measured with a potentiostatic electrochemical impedance spectrometer (Solartron, 1255 HF Frequency Response Analyzer) at 10 kHz. All electrochemical data was collected vs. Ag/AgCl reference. The *iR*-compensated potentials relative to the reversible hydrogen electrode (RHE) are shown in the tables in the supporting information using the following equations:

$$V_{\text{comp}}(\text{Ag/AgCl}) = V_{\text{app}}(\text{Ag/AgCl}) + iR$$

$$V_{\text{comp}}(\text{RHE}) = V_{\text{comp}}(\text{Ag/AgCl}) + 0.197 + 0.059 \cdot \text{pH}$$

Liquid-phase products in the catholyte were collected for quantification using nuclear magnetic resonance (NMR).

Product analysis. The reduction compartment of the gas-tight reactor was connected to the inlet of the sample loop of a gas chromatograph (GC, Buck Scientific, Model 910). GC measurements were performed on sample injections taken after 10 and 38 min of the CO₂RR to determine the concentration of gaseous products present: CO, CH₄, C₂H₄, H₂. The GC was equipped with a methanizer and a flame ionization detector (FID) to detect CO and hydrocarbons and a thermal

conductivity detector (TCD) to detect H₂. Nitrogen was used as the carrier gas. Liquid products were quantified using 1D ¹H NMR (400 MHz, Bruker high field NMR spectrometers). Each sample of catholyte (700 μL) was mixed with 35 μL of a D₂O solution containing internal standards: 50 mM phenol and 10 mM dimethyl sulfoxide (DMSO). The water peak was suppressed by a WET procedure (Bruker). The acquired NMR data were processed with Topspin 4.0.5 software. The peak area of the liquid product (formate) at higher chemical shift with respect to the suppressed water peak (chemical shift = 4.7 ppm) was normalized to the peak area of phenol (chemical shift = 7.2 ppm). The peak areas of the liquid products (acetate, ethanol, propanol, acetaldehyde, propionaldehyde, glycolaldehyde, and allyl alcohol) at lower chemical shift with respect to the suppressed water peak were normalized to the peak area of DMSO (chemical shift = 2.6 ppm).

Data availability

The data supporting the findings of this study are available within the article and Supplementary Information file. All other relevant source data are available from the corresponding author upon request. The source data underlying Figs. 2, 4–7 and Supplementary Figs. 1, 2, 9–15, 18, and 19 are provided as a Source data file.

Received: 21 July 2019; Accepted: 29 May 2020;

Published online: 17 July 2020

References

- Sawyer, J. S. Man-made carbon dioxide and the “greenhouse” effect. *Nature* **239**, 23–26 (1972).
- Xu, Y., Ramanathan, V. & Victor, D. G. Global warming will happen faster than we think. *Nature* **564**, 30–32 (2018).
- Hori, Y. In *Modern Aspects of Electrochemistry* Vol. 42 (eds Vayenas, C. G., White, R. E. & Gambaio-Aldaco, M. E.) 89–189 (Springer, 2008).
- Gattrell, M., Gupta, N. & Co, A. A review of the aqueous electrochemical reduction of CO₂ to hydrocarbons at copper. *J. Electroanal. Chem.* **594**, 1–19 (2006).
- Kuhl, K. P., Cave, E. R., Abram, D. N. & Jaramillo, T. F. New insights into the electrochemical reduction of carbon dioxide on metallic copper surfaces. *Energy Environ. Sci.* **5**, 7050–7059 (2012).
- Nitopi, S. et al. Progress and perspectives of electrochemical CO₂ reduction on copper in aqueous electrolyte. *Chem. Rev.* **119**, 7610–7672 (2019).
- Kibria, M. G. et al. Electrochemical CO₂ reduction into chemical feedstocks: from mechanistic electrocatalysis models to system design. *Adv. Mater.* **31**, 1807166 (2019).
- Hori, Y., Wakebe, H., Tsukamoto, T. & Koga, O. Electrocatalytic process of CO selectivity in electrochemical reduction of CO₂ at metal electrodes in aqueous media. *Electrochim. Acta* **39**, 1833–1839 (1994).
- Sen, S., Liu, D. & Palmore, G. T. R. Electrochemical reduction of CO₂ at copper nanofoams. *ACS Catal.* **4**, 3091–3095 (2014).
- Kim, D., Kley, C. S., Li, Y. & Yang, P. Copper nanoparticle ensembles for selective electroreduction of CO₂ to C₂–C₃ products. *Proc. Natl Acad. Sci. USA* **114**, 10560–10565 (2017).
- Li, C. W. & Kanan, M. W. CO₂ reduction at low overpotential on Cu electrodes resulting from the reduction of thick Cu₂O films. *J. Am. Chem. Soc.* **134**, 7231–7234 (2012).
- Mistry, H. et al. Highly selective plasma-activated copper catalysts for carbon dioxide reduction to ethylene. *Nat. Commun.* **7**, 12123 (2016).
- Gao, D. et al. Plasma-activated copper nanocube catalysts for efficient carbon dioxide electroreduction to hydrocarbons and alcohols. *ACS Nano* **11**, 4825–4831 (2017).
- Roberts, F. S., Kuhl, K. P. & Nilsson, A. High selectivity for ethylene from carbon dioxide reduction over copper nanocube electrocatalysts. *Angew. Chem. Int. Ed.* **54**, 5179–5182 (2015).
- Loidice, A. et al. Tailoring copper nanocrystals towards C₂ products in electrochemical CO₂ reduction. *Angew. Chem. Int. Ed.* **55**, 5789–5792 (2016).
- Li, Y. et al. Structure-sensitive CO₂ electroreduction to hydrocarbons on ultrathin 5-fold twinned copper nanowires. *Nano Lett.* **17**, 1312–1317 (2017).
- Raciti, D., Mao, M., Park, J. H. & Wang, C. Local pH effect in the CO₂ reduction reaction on high-surface-area copper electrocatalysts. *J. Electrochem. Soc.* **165**, F799–F804 (2018).
- Zhang, H. et al. Cu nanowire-catalyzed electrochemical reduction of CO or CO₂. *Nanoscale* **11**, 12075–12079 (2019).
- Kibria, M. G. et al. A surface reconstruction route to high productivity and selectivity in CO₂ electroreduction toward C₂₊ hydrocarbons. *Adv. Mater.* **30**, 1804867 (2018).
- Hori, Y., Takahashi, I., Koga, O. & Hoshi, N. Electrochemical reduction of carbon dioxide at various series of copper single crystal electrodes. *J. Mol. Catal. A Chem.* **199**, 39–47 (2003).
- Huang, Y., Handoko, A. D., Hirunsit, P. & Yeo, B. S. Electrochemical reduction of CO₂ using copper single-crystal surfaces: effects of CO* coverage on the selective formation of ethylene. *ACS Catal.* **7**, 1749–1756 (2017).
- Gupta, N., Gattrell, M. & MacDougall, B. Calculation for the cathode surface concentrations in the electrochemical reduction of CO₂ in KHCO₃ solutions. *J. Appl. Electrochem.* **36**, 161–172 (2006).
- Peterson, A. A., Abild-Pedersen, F., Studt, F., Rossmeisl, J. & Nørskov, J. K. How copper catalyzes the electroreduction of carbon dioxide into hydrocarbon fuels. *Energy Environ. Sci.* **3**, 1311–1315 (2010).
- Nie, X., Esopi, M. R., Janik, M. J. & Asthagiri, A. Selectivity of CO₂ reduction on copper electrodes: the role of the kinetics of elementary steps. *Angew. Chem. Int. Ed.* **52**, 2459–2462 (2013).
- Durand, W. J., Peterson, A. A., Studt, F., Abild-Pedersen, F. & Nørskov, J. K. Structure effects on the energetics of the electrochemical reduction of CO₂ by copper surfaces. *Surf. Sci.* **605**, 1354–1359 (2011).
- Goodpaster, J. D., Bell, A. T. & Head-Gordon, M. Identification of possible pathways for C–C bond formation during electrochemical reduction of CO₂: new theoretical insights from an improved electrochemical model. *J. Phys. Chem. Lett.* **7**, 1471–1477 (2016).
- Sandberg, R. B., Montoya, J. H., Chan, K. & Nørskov, J. K. CO–CO coupling on Cu facets: Coverage, strain and field effects. *Surf. Sci.* **654**, 56–62 (2016).
- Calle-Vallejo, F. & Koper, M. T. Theoretical considerations on the electroreduction of CO to C₂ species on Cu (100) electrodes. *Angew. Chem. Int. Ed.* **52**, 7282–7285 (2013).
- Kortlever, R., Shen, J., Schouten, K. J. P., Calle-Vallejo, F. & Koper, M. T. Catalysts and reaction pathways for the electrochemical reduction of carbon dioxide. *J. Phys. Chem. Lett.* **6**, 4073–4082 (2015).
- Pérez-Gallent, E., Figueiredo, M. C., Calle-Vallejo, F. & Koper, M. T. Spectroscopic observation of a hydrogenated CO dimer intermediate during CO reduction on Cu (100) electrodes. *Angew. Chem. Int. Ed.* **129**, 3675–3678 (2017).
- Xiao, H., Cheng, T., Goddard, W. A. III & Sundaraman, R. Mechanistic explanation of the pH dependence and onset potentials for hydrocarbon products from electrochemical reduction of CO on Cu (111). *J. Am. Chem. Soc.* **138**, 483–486 (2016).
- Liu, X. et al. pH effects on the electrochemical reduction of CO₍₂₎ towards C₂ products on stepped copper. *Nat. Commun.* **10**, 32 (2019).
- Cheng, T., Xiao, H. & Goddard, W. A. Nature of the active sites for CO reduction on copper nanoparticles; suggestions for optimizing performance. *J. Am. Chem. Soc.* **139**, 11642–11645 (2017).
- Lum, Y. & Ager, J. W. Stability of residual oxides in oxide-derived copper catalysts for electrochemical CO₂ reduction investigated with ¹⁸O labeling. *Angew. Chem. Int. Ed.* **57**, 551–554 (2018).
- Cavalca, F. et al. Nature and distribution of stable subsurface oxygen in copper electrodes during electrochemical CO₂ reduction. *J. Phys. Chem. C* **121**, 25003–25009 (2017).
- Eilert, A. et al. Subsurface oxygen in oxide-derived copper electrocatalysts for carbon dioxide reduction. *J. Phys. Chem. Lett.* **8**, 285–290 (2016).
- Favaro, M. et al. Subsurface oxide plays a critical role in CO₂ activation by Cu (111) surfaces to form chemisorbed CO₂, the first step in reduction of CO₂. *Proc. Natl Acad. Sci. USA* **114**, 6706–6711 (2017).
- Xiao, H., Goddard, W. A., Cheng, T. & Liu, Y. Cu metal embedded in oxidized matrix catalyst to promote CO₂ activation and CO dimerization for electrochemical reduction of CO₂. *Proc. Natl Acad. Sci. USA* **114**, 6685–6688 (2017).
- Fields, M., Hong, X., Nørskov, J. K. & Chan, K. Role of subsurface oxygen on Cu surfaces for CO₂ electrochemical reduction. *J. Phys. Chem. C* **122**, 16209–16215 (2018).
- Garza, A. J., Bell, A. T. & Head-Gordon, M. Is subsurface oxygen necessary for the electrochemical reduction of CO₂ on copper? *J. Phys. Chem. Lett.* **9**, 601–606 (2018).
- Chen, C. S. et al. Stable and selective electrochemical reduction of carbon dioxide to ethylene on copper mesocrystals. *Catal. Sci. Technol.* **5**, 161–168 (2015).
- Kwon, Y., Lum, Y., Clark, E. L., Ager, J. W. & Bell, A. T. CO₂ electroreduction with enhanced ethylene and ethanol selectivity by nanostructuring polycrystalline copper. *ChemElectroChem* **3**, 1012–1019 (2016).
- Bianchi, G. & Longhi, P. Copper in sea-water, potential-pH diagrams. *Corros. Sci.* **13**, 853–864 (1973).
- King, F., Lilja, C., Pedersen, K., Pitkänen, P. & Vähänen, M. *An Update Of The State-of-the-art Report On The Corrosion Of Copper Under Expected Conditions In A Deep Geologic Repository* (Swedish Nuclear Fuel and Waste Management Co., 2010).
- Ahrland, S., Chatt, J. & Davies, N. The relative affinities of ligand atoms for acceptor molecules and ions. *Q. Rev. Chem. Soc.* **12**, 265–276 (1958).
- Ahrland, S., Tagesson, B. & Tuhtar, D. Thermodynamics of metal complex formation in aqueous solution. XIII. Enthalpy measurements on copper (I) and silver (I) halide systems. *Acta Chem. Scand., Ser. A* **31**, 625 (1977).

47. Xu, H., Wang, W. & Zhu, W. Shape evolution and size-controllable synthesis of Cu₂O octahedra and their morphology-dependent photocatalytic properties. *J. Phys. Chem. B* **110**, 13829–13834 (2006).
48. McCrum, I. T., Akhade, S. A. & Janik, M. J. Electrochemical specific adsorption of halides on Cu 111, 100, and 211: A Density Functional Theory study. *Electrochim. Acta* **173**, 302–309 (2015).
49. Pourbaix, M. *Atlas of Electrochemical Equilibria in Aqueous Solutions* (National Association of Corrosion Engineers, 1974).
50. Singh, M. R., Kwon, Y., Lum, Y., Ager, J. W. III & Bell, A. T. Hydrolysis of electrolyte cations enhances the electrochemical reduction of CO₂ over Ag and Cu. *J. Am. Chem. Soc.* **138**, 13006–13012 (2016).
51. Chen, C. S., Wan, J. H. & Yeo, B. S. Electrochemical reduction of carbon dioxide to ethane using nanostructured Cu₂O-derived copper catalyst and palladium (II) chloride. *J. Phys. Chem. C* **119**, 26875–26882 (2015).
52. Wang, H. et al. Rapid and scalable synthesis of cuprous halide-derived copper nano-architectures for selective electrochemical reduction of carbon dioxide. *Nano Lett.* **19**, 3925–3932 (2019).

Acknowledgements

This research was supported in part by the Center for the Capture and Conversion of CO₂, a Center for Chemical Innovation funded by the National Science Foundation, CHE-1240020 and seed funding from Brown University. The authors thank Anthony McCormick and Hector Garces for assistance with SEM, EDS, and XRD instrumentation in the advanced instrumentation facilities at Brown University, Seunghee Han (KIST) for help with argon ion implantation, and Byoung Koun Min, Yun Jeong Hwang, Hyewon Yoon, Yongjun Choi, Sungmin Park, Hae Jung Son, and Doh-Kwon Lee (KIST) for enabling additional experiments to address reviewer comments.

Author contributions

T.K. designed and performed the experiments. G.T.R.P. supervised the project. T.K. and G.T.R.P. analyzed and discussed the data and prepared the paper.

Competing interests

The authors declare no competing interests.

Additional information

Supplementary information is available for this paper at <https://doi.org/10.1038/s41467-020-16998-9>.

Correspondence and requests for materials should be addressed to G.T.R.P.

Peer review information *Nature Communications* thanks Feng Jiao, Anders Nilsson, and other, anonymous reviewers for their contributions to the peer review of this work.

Reprints and permission information is available at <http://www.nature.com/reprints>

Publisher's note Springer Nature remains neutral with regard to jurisdictional claims in published maps and institutional affiliations.



Open Access This article is licensed under a Creative Commons Attribution 4.0 International License, which permits use, sharing, adaptation, distribution and reproduction in any medium or format, as long as you give appropriate credit to the original author(s) and the source, provide a link to the Creative Commons license, and indicate if changes were made. The images or other third party material in this article are included in the article's Creative Commons license, unless indicated otherwise in a credit line to the material. If material is not included in the article's Creative Commons license and your intended use is not permitted by statutory regulation or exceeds the permitted use, you will need to obtain permission directly from the copyright holder. To view a copy of this license, visit <http://creativecommons.org/licenses/by/4.0/>.

© The Author(s) 2020